

# Automated Evaluation of Power Plant Frequency and Voltage Control using Synchrophasors

Jim Follum  
Pacific Northwest National Laboratory  
[james.follum@pnnl.gov](mailto:james.follum@pnnl.gov)

Priya Mana  
Pacific Northwest National Laboratory  
[priya.mana@pnnl.gov](mailto:priya.mana@pnnl.gov)

Elliott Mitchell-Colgan  
Bonneville Power Administration  
[ejmitchell-colgan@bpa.gov](mailto:ejmitchell-colgan@bpa.gov)

Anthony Faris  
Bonneville Power Administration  
[ajfaris@bpa.gov](mailto:ajfaris@bpa.gov)

## Abstract

*Reliable power system operation depends on maintaining acceptable frequency and voltage. When excursions occur, power plants must respond appropriately to restore these parameters within a suitable margin of their nominal values. Model-based post event analysis is useful for ensuring that power plant controls are functioning properly, but these analyses are labor intensive. To address this challenge, this paper proposes automated measurement-based approaches for detecting excursions and evaluating the frequency and voltage control performance of power plants as they respond. The performance of a power plant is quantified using a novel voltage response measure and a modified frequency response measure applicable to an individual power plant. These metrics gauge how much each power plant adjusts active or reactive power injection to restore frequency or voltage. The detection and analysis methods are validated using publicly available field measurements and the results from a field demonstration at Bonneville Power Administration (BPA). The field demonstration verified that the metrics effectively summarize a power plant's performance, allowing further review of plants with potential deficiencies.*

## 1. Introduction

One of the critical aspects of reliable power system operation is maintaining acceptable frequency and voltage. Following grid disturbances, this is

accomplished by power plants that adjust their active and reactive power output to restore frequency and voltage. Without these local controls it would be difficult for large power systems to maintain frequency and voltage stability [1].

To ensure that bulk power systems can provide sufficient response following a loss of generation, the North American Electric Reliability Corporation (NERC) mandates that balancing authorities provide sufficient frequency response [2]. A balancing authority's frequency response is a measure of how much additional active power the generators within their territory provide following a sudden decrease in frequency. Along with this performance requirement, NERC mandates that models be verified to ensure that they accurately reflect the capabilities of generators to maintain frequency through adjustment of active power [3] and voltage through adjustment of reactive power [4].

To ensure their adherence to these standards, the Bonneville Power Administration (BPA), a balancing authority in the Northwest United States, regularly compares the measured response of power plants in their territory to a simulated response. If the measured active and reactive power agree with the simulated values, it confirms that the power plant's controls are performing as expected. Though this approach is effective, it requires each excursion to be selected and analyzed manually using custom scripts. Complementary approaches based exclusively on measurements have been developed to reduce this burden.

High-speed time-synchronized measurements called synchrophasors [5] are particularly useful for these analyses. As discussed in [6], BPA uses the open-source Frequency Response and Analysis Tool (FRAT) [7] to analyze their system's response to under-frequency

---

The Pacific Northwest National Laboratory is operated for the U.S. Department of Energy by Battelle Memorial Institute under Contract DE-AC05-76RL01830. This work was funded by the U.S. DOE.

excursions. Less work has been done to evaluate voltage control performance using synchrophasors, but recent publications have shown that low-order models can be used to evaluate the performance of STATCOMs under ambient and disturbance conditions [8] and wind turbine generators following disturbances [9].

To further reduce the burden of performance evaluation, BPA collaborated with the Pacific Northwest National Laboratory (PNNL) to develop the *Generator Scorecard* tool. Images of the tool's user interface, which is not the focus of this paper, can be found in [10]. The tool analyzes synchrophasor measurements to detect frequency and voltage excursions and then automatically evaluates the active and reactive power response of power plants. The performance is quantified in frequency and voltage response measures that can help identify under-performing plants for further model-based review. The paper discusses the applications developed as a part of the *Generator Scorecard* to observe and quantify power plant performance during frequency and voltage excursions through a frequency response measure (FRM) and voltage response measure (VRM). These applications and the associated procedure to implement them by extracting useful information from synchrophasor data are shown in Fig. 1. The sections of the paper corresponding to each step in the analysis are noted in parentheses.

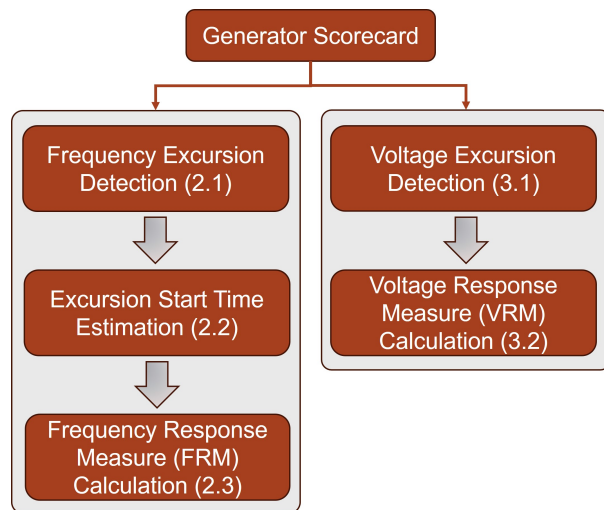


**Figure 1. Overview of the Generator Scorecard applications. The paper's section corresponding to each step in the analysis is noted in parentheses.**

The key contributions of this paper are detailed descriptions of the algorithms needed to automatically calculate frequency and voltage response measures by detecting and analyzing excursions. The formula for the

VRM is a novel contribution of this paper. The formula captures how a power plant adjusts reactive power to moderate the sudden change in voltage magnitude that occurs after a capacitor is switched in or out of the system. Simulation results are used to motivate the formula and illustrate how it can be used to identify a problem in a power plant's control. To support the VRM's calculation, a detection algorithm for capacitor switching events is proposed. Results from a field demonstration at BPA are used to validate the approaches.

The FRM for a particular power plant is similar to the FRM defined by NERC for application to balancing authorities [2]. The novelty of the Generator Scorecard is in the frequency excursion detector and start time estimator that enable automation. The detector utilizes a low-pass filter to extract the signal components of interest, which is crucial for addressing the complexities found in real-world measurements. The detector extends traditional under-frequency excursion analysis by also detecting over-frequency excursions due to large motors in pumped storage hydro facilities turning off. These excursions have previously been used for inertia estimation [11]. Over-frequency events are important to consider because some power plants, particularly renewable resources, are operated without reserves [1]. These resources may have appropriately configured frequency controls, but with no headroom they cannot respond to under-frequency excursions. Thus, over-frequency excursions are needed to determine if the frequency control is active.

To calculate the FRM for a detected excursion, the event's start time must be estimated. This paper explains how this time can be estimated for both under- and over-frequency excursions. The estimator for under-frequency excursion start times is based on the step response of a low-pass filter. This paper provides a more detailed description of the algorithm than the overview in [12], which focused on highlighting use cases for the publicly available Grid Event Signature Library (GESL) [13, 14]. Using events from this library, [12] showed that the excursion start time estimator outperformed a baseline approach deployed in the FRAT tool. A more comprehensive analysis of the performance of the detector and start time estimator based on GESL events is provided in this paper. These events are publicly available, making the results reproducible for those that wish to implement or improve upon the proposed algorithms. Results from a field demonstration at BPA are also presented.

The rest of the paper is organized as follows. The FRM and its supporting algorithms are described in Section 2 followed by VRM analysis in Section 3.

Results based on field-measured data are reviewed for FRM and VRM in Sections 4 and 5, respectively. Concluding remarks and expectations for future work are provided in Section 6.

## 2. FRM Methodology

The automated approach to frequency response analysis proposed in this paper involves detecting a frequency excursion and then estimating its start time. Once the start time is known, the FRM can be calculated by applying a simple formula to the appropriate measurements of frequency and active power. The detector and start time estimator are described in Sections 2.1 and 2.2, respectively. The FRM formula and its calculation are described in Section 2.3.

### 2.1. Frequency Excursion Detection

The proposed excursion detector considers both the size of frequency deviations and how rapidly they occur. Denote the input frequency measurements as  $F(k)$  where  $k$  is the sample index. These input measurements have the nominal 60 Hz component removed by subtracting the first sample from all subsequent measurements. This adjustment prepares the signal for the first step in the detector, the application of a low-pass filter to limit the measurements to the large trends of interest. A Parks-McClellan finite impulse response (FIR) filter was designed for this purpose with a passband ripple of 0.05 dB, 50 dB of attenuation in the stopband, and a transition band from 0.22 Hz to 0.28 Hz. With an order of 1311 (2622) for PMU data at 30 (60) samples per second, the filter's group delay was 21.85 seconds. Because the filter is linear phase, this group delay is simple to account for when reporting the timing of an excursion. Denote the filtered frequency signal as  $\tilde{F}(k)$  where the group delay has been accounted for so that  $\tilde{F}(k)$  corresponds to  $F(k)$ . An example of  $F(k)$  and  $\tilde{F}(k)$  from the publicly available Grid Event Signature Library (GESL) is provided in Fig. 2.

Next, let  $m \in k$  denote the set of indices such that  $\tilde{F}(m)$  are the maxima and minima of  $\tilde{F}(k)$ . These extrema are indicated by red dots in Fig. 2. The slopes between them can then be expressed in Hz per second as

$$S(m) = \frac{\Delta[\tilde{F}(m)]}{\Delta[m]} f_s \quad (1)$$

where  $f_s$  is the sample rate and the operator  $\Delta[\cdot]$  returns the difference between the input and the next value in the series. The slopes for the example in Fig. 2 are displayed in Fig. 3.

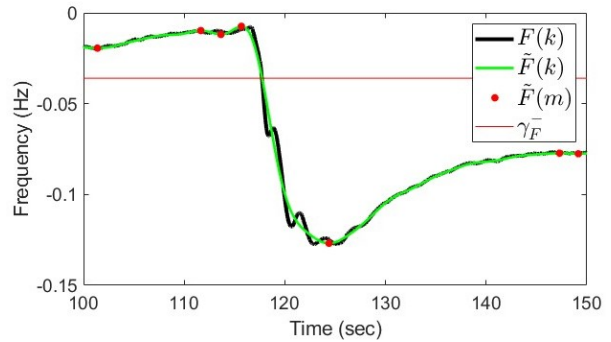


**Figure 2. Example of the excursion detector applied to signature 2031 listed under Provider 10 in the GESL.**

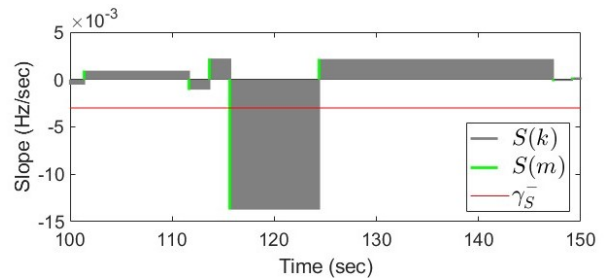


**Figure 3. Slopes associated with the frequency event in Fig. 2.**

To allow for detection at all samples, let  $S(k)$  equal the nearest value of  $S(m)$  for which  $k \geq m$ . In this way, the slope is associated with all samples between two extrema. These values are indicated by the gray blocks in Fig. 3.

An over-frequency excursion is detected when the frequency and its slope exceed thresholds:

$$(\tilde{F}(k) > \gamma_F^+) \cap (S(k) > \gamma_S^+). \quad (2)$$

Similarly, an under-frequency excursion is detected when the frequency and its slope drop below thresholds:

$$(\tilde{F}(k) < \gamma_F^-) \cap (S(k) < \gamma_S^-). \quad (3)$$

Here  $\gamma_F$  and  $\gamma_S$  are thresholds for the frequency and slope, respectively, and the  $\pm$  superscripts indicate whether the threshold is for over- or under-frequency excursions. Based on discussions with BPA, the frequency thresholds were set to  $\gamma_F = \pm 0.036$  Hz for this study. The value of 0.036 Hz was selected based on the maximum deadband setting for the Western Interconnection listed in NERC's reliability guideline for primary frequency control [15]. The slope thresholds were selected empirically as  $\gamma_S = \pm 0.003$  Hz per second. The thresholds are exceeded in Figs. 2 and 3,

so this event satisfies (3). Thus, this excursion would be detected with the proposed method.

## 2.2. Estimation of Excursion Start Time

Once an excursion is detected, the time when the excursion began, denoted as  $t_0$ , must be estimated. For the over-frequency excursions considered in this study, the start time coincided with the final minima before detection occurred, as depicted in Fig. 4.

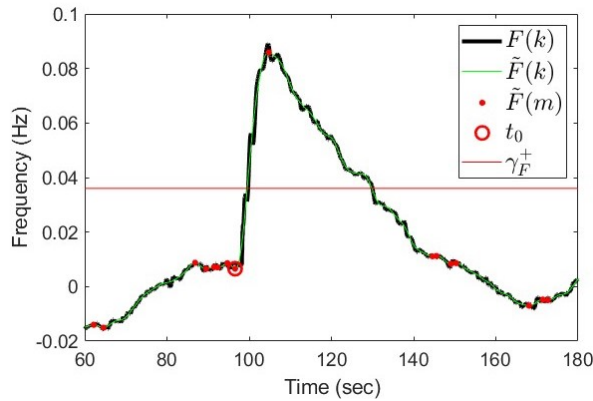


**Figure 4. Example of excursion detection and start time estimation for signature 2012 listed under Provider 10 in the GESL.**

To handle the greater variety and complexity of under-frequency excursions, a more involved process for estimating  $t_0$  was developed. To begin, a low-pass filter is applied to the input signal  $F(k)$ , which produces the signal  $\hat{F}(k)$ . The filter is applied in the forward and reverse directions to achieve zero phase distortion, a process known as zero-phase filtering. With this approach, there is no need to adjust for group delay. The FIR filter was designed using the Kaiser window method with a shape parameter of  $\beta = 5$  and a cutoff frequency of  $1/(2f_s)$  Hz. The filter's order was 1200 (2400) for signals at 30 (60) samples per second. The response of this filter to a downward step is displayed in Fig. 5. As described next, the characteristic overshoot followed by a gradual decline was useful in developing an estimation method for  $t_0$ .

To illustrate this approach, the original and filtered signals from the same event in Fig. 2 are presented in the top plot of Fig. 6. After applying the filter, the first-order derivative is calculated, as displayed in the bottom plot of Fig. 6. The derivative's minimum during the period when  $\hat{F}(k) < \gamma_F^-$  establishes the rightmost boundary indicated by a vertical dotted line in Fig. 6. The boundary to the left is then selected as the point preceding the minimum where the derivative was last positive. The points  $X_1$  and  $X_2$  are the first and last

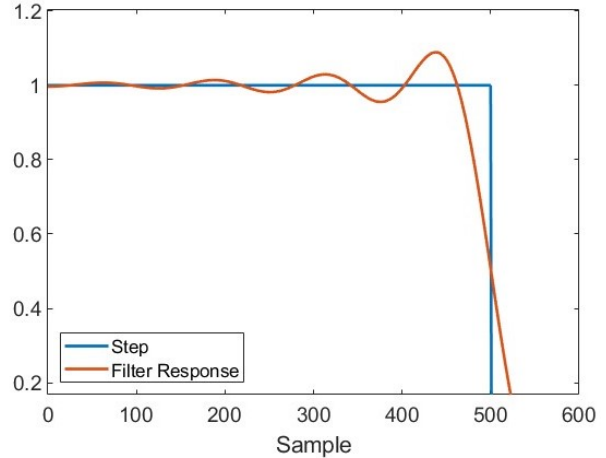


**Figure 5. Response of the low-pass filter used for start time estimation to a downward step.**

samples within these boundaries where  $\hat{F}(k) < F(k)$ . Finally, the excursion's starting point is estimated as the point where the difference between the original and low-pass filtered frequencies is largest:

$$t_0 = \underset{k}{\operatorname{argmax}} (F(k) - \hat{F}(k)) , X_1 < k < X_2. \quad (4)$$

With  $t_0$  estimated, the frequency response of a power

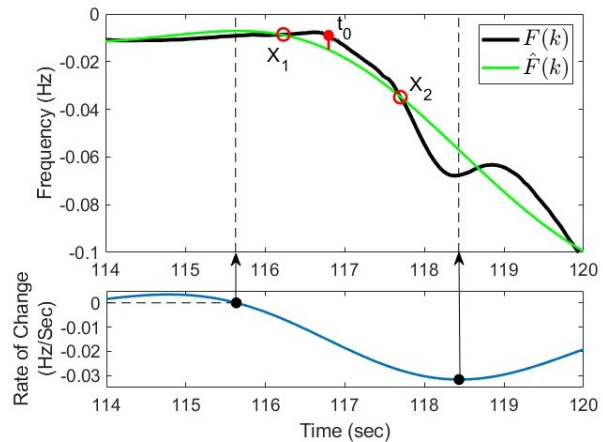


**Figure 6. Example of excursion detection and start time estimation for signature 2012 listed under Provider 10 in the GESL.**

plant can be evaluated, as discussed next.

## 2.3. Frequency Response Measure Calculation

The values defined by NERC's BAL-003-1 standard [2] for use in frequency response analysis are displayed in Fig. 7. These measurements are from the first PMU in

the GESL signature 2463 under Provider 10. Though it cannot be confirmed that the active power measurements represent the output from a power plant, they resemble the measurements from known power plants in the study presented in Section 4.2. Here, they are used only for illustration. For both frequency and power,  $A$  is the average of measurements for the 16 seconds leading up to  $t_0$  and  $B$  is the average from 20 to 52 seconds after  $t_0$ . For this study, the same definitions were used for under- and over-frequency excursions. The nadir point  $C$  was selected as the minimum or maximum frequency measurement (depending on the excursion type) for the 20 seconds after  $t_0$ .

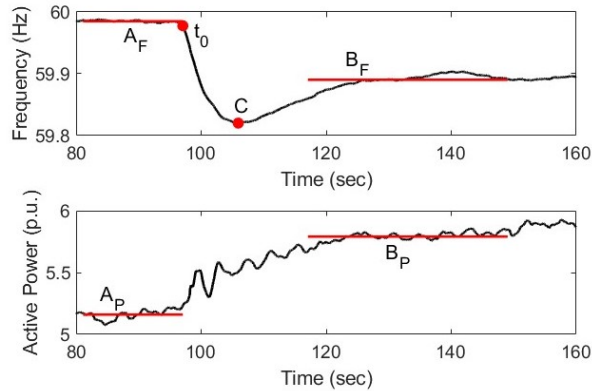


**Figure 7. Illustration of the inputs to the FRM calculation for Signature 2463 under Provider 10 in the GESL.**

Once  $A$ ,  $B$ , and  $C$  are determined, they are evaluated to ensure that only events of interest are analyzed further. Specifically, if the maximum frequency between  $C$  and  $B$  is greater than  $A_F$  for an under-frequency excursion, the event is likely a transient oscillation that should not be considered. Thus, only events for which

$$\max(F(k_C, k_C + 1, \dots, k_{t_0+20})) < A_F \quad (5)$$

are retained. Additionally, under-frequency excursions must satisfy

$$A_F > B_F \quad (6)$$

and over-frequency excursions must satisfy

$$A_F < B_F \quad (7)$$

to ensure that the events have the characteristic shapes depicted in Figs. 2 and 4.

For events passing these checks, the frequency response measure for the plant is calculated as

$$FRM = \frac{B_P - A_P}{10(B_F - A_F)} \quad (8)$$

with units of MW/0.1Hz. This formula closely reflects the formula for a balancing authority's FRM derived in [2], except that only a single plant is considered. Negative values of the FRM are desirable. The numerator is negative for under-frequency excursions, so an increase in active power is desired to increase the frequency. Conversely, the numerator is positive for over-frequency events where a decrease in active power will decrease the system's frequency. Larger FRM values indicate that the plant is making a larger contribution to returning the frequency to nominal.

### 3. VRM Methodology

The voltage response measure quantifies a power plant's adjustment of reactive power following a sudden change in the voltage magnitude at the plant's point of interconnection. In this way, the VRM indicates whether a plant is supporting the power system's voltage stability by providing reactive power support. The voltage excursion detector used to find capacitor switching events for analysis is described in Section 3.1, followed by an explanation of the VRM's calculation in Section 3.2.

#### 3.1. Voltage Excursion Detection

The voltage excursion detector's operation, which is depicted in Fig. 8, is based on setting a limit for the amount of time the voltage magnitude remains outside of lower and upper thresholds. Denoting the thresholds for voltage magnitude  $V(k)$  as  $\gamma_V^-$  and  $\gamma_V^+$ , define an indicator function

$$I(k) = \begin{cases} 0 & \gamma_V^- \leq V(k) \leq \gamma_V^+ \\ 1 & \text{Otherwise} \end{cases} \quad (9)$$

where  $k$  spans the most recent  $K$  samples. Detection occurs when the voltage remains outside of its thresholds for  $\gamma_I$  of the most recent  $K$  samples:

$$\sum_{k=1}^K I(k) \geq \gamma_I. \quad (10)$$

For the results presented in Section 5,  $\gamma_I$  and  $K$  were set to the equivalent of 30 and 35 seconds, respectively.

The thresholds  $\gamma_V^-$  and  $\gamma_V^+$  were continuously updated by applying negative and positive deviations to a baseline value. For the results in this paper, the baseline was established by averaging the most recent 180 seconds of measurements. The change in voltage magnitude caused by capacitor switching differs between locations in the power system, so the deviations

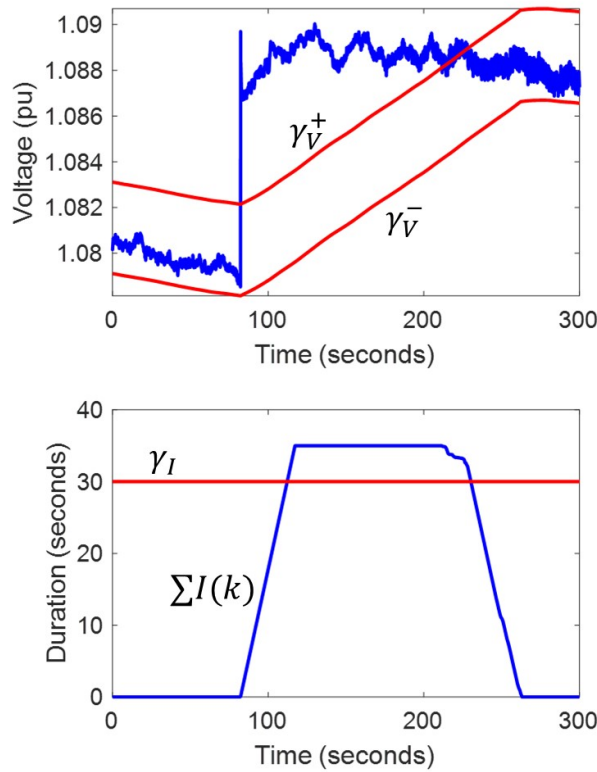


Figure 8. Example of the voltage excursion detector's operation with a voltage exceeding its upper threshold (top) for more than the 30-second threshold for duration (bottom).

were chosen based on a review of measurements at each location of interest. The selected deviations varied across these locations from 0.5 to 2.1 kV line-to-line.

### 3.2. Voltage Response Measure

To motivate the VRM and illustrate its calculation, a wind power plant's response to a capacitor switching event was simulated. The simulation was performed by playing real voltage and frequency measurements from the point of interconnection into a collector system model that includes an aggregate generator. The input voltage and reactive power response are presented in Fig. 9. The values  $A_V$  and  $A_Q$  are the five-second averages of voltage and reactive power prior to the capacitor switching. The points  $C_V$  and  $C_Q$  mark the beginning of the plant's response in reactive power. They correspond to the point immediately after the voltage magnitude rebounds from its most extreme value. The settling values are denoted as  $B_V$  and  $B_Q$  and are the averages from two to four seconds after  $C_V$  and  $C_Q$ .

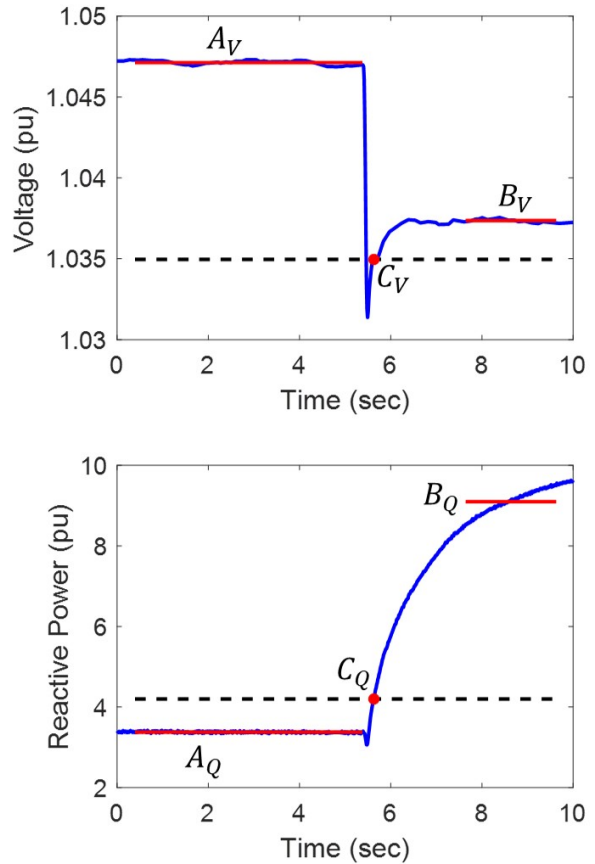


Figure 9. Simulation of a wind power plant's appropriate response in reactive power (bottom) to a sudden change in voltage at the point of interconnection (top).

Following the drop in voltage due to the capacitor switching out, the plant's response in reactive power is quantified as  $B_Q - C_Q$ . This response contributes to the desired increase in voltage, quantified as  $B_V - C_V$ . Multiplying these terms results in a large value when the plant provides a strong response, leading to the metric

$$VRM = \frac{B_Q - C_Q}{|C_Q - A_Q|} \times \frac{B_V - C_V}{|C_V - A_V|}. \quad (11)$$

The scaling terms in the denominators help provide consistent values at points in the system with different nominal voltages and levels of stiffness. The scaling also cancels the units, so the VRM is a scalar. Large positive values are desirable, indicating that reactive power increased to boost voltage or reactive power decreased to bring down the voltage. For the response in Fig. 9, the VRM is 1.17.

To illustrate how the VRM can identify under-performing plants, the *reflflag* and *qref* parameters

in the *repc\_a* [16] model of the plant's controller were set to zero. These changes reflect the situation where a plant is not operating in voltage-control mode, something that occurs on occasion in real power systems. The simulation was then rerun with the same field measurements of frequency and voltage played in at the point of interconnection, resulting in the reactive power output displayed in Fig. 10. As expected, the change in reactive power is much smaller than in Fig. 9. The degraded performance is reflected in a much lower VRM of 0.07. Identifying this type of performance issue quickly was one of the motivations for development of the Generator Scorecard tool.

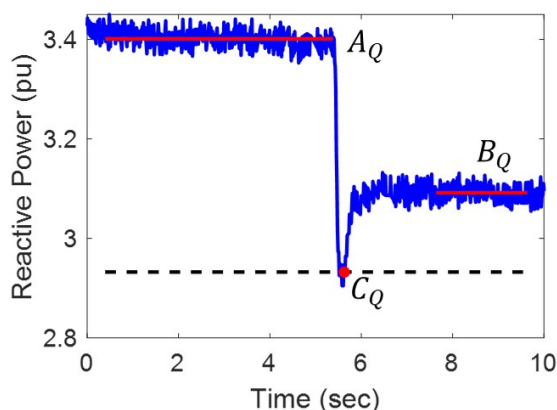


**Figure 10. Simulation of a power plant's poor response to the sudden change in voltage in Fig. 9.**

## 4. FRM Results and Analysis

This section evaluates all aspects of automated FRM calculation using field-measured data. Frequency excursion measurements from a public library are first analyzed in Section 4.1 so that others can reproduce the results and improve upon them. Results from the Generator Scorecard's field demonstration at BPA are then discussed in Section 4.2.

### 4.1. Results from a Public Data Library

The results in this section are based on a public repository of power system measurements called the Grid Event Signature Library (GESL) [13]. Specifically, signatures listed under the GESL's Provider 10, which corresponds to measurements from the Western Interconnection of North America, were analyzed in preparation for field testing at BPA. Though the measurements may not be from BPA, the frequency signals from across an interconnection can be expected

to have similar characteristics. Details of the Provider 10 dataset can be found in [14].

For this study, the 237 signatures with tags *Events::System Event/Condition::Frequency Deviation* were analyzed. These signatures include a variety of events that perturbed the system's frequency and were not limited to the under- and over-frequency excursions of interest. Some signatures include both types of excursions. Applying the detection algorithm in Section 2.1 and the checks in (5)-(7) resulted in 105 under-frequency excursions, 3 over-frequency excursions, and 131 events that were automatically deemed unsuitable for FRM analysis.

The vast majority of unsuitable events were transients. A smaller portion were discarded by the checks in (5)-(7) or were excursions that were too small or too slow moving to be detected. Tighter thresholds would lead to detection of these events, but the overall results indicate that the thresholds are appropriate for this use case.

A visual review indicated that all of the over- and under-frequency excursions were correctly identified as events of interest and that the estimation of  $t_0$  was highly successful. To quantify performance for the more numerous under-frequency excursions,  $t_0$  was assigned based on visual inspection. The resulting values of  $A_F$  and  $B_F$  were then compared with those based on estimates of  $t_0$  from the algorithm proposed in Section 2.2. The median absolute error for  $A_F$  and  $B_F$  were quite small at 0.045 mHz and 0.083 mHz, respectively. Of the 105 cases, there were two where the algorithm selected start times distinctly different than the points selected based on visual inspection. As can be seen on the GESL website, Signature ID 2481 has a very gradual frequency decline and Signature ID 2496 has large swings as the frequency declines. These peculiarities make automatic estimation of the excursion start time challenging. To handle such cases, the Generator Scorecard tool allows manual adjustment of  $t_0$ .

### 4.2. Results from Field Demonstration

After initial development, the FRM and VRM analytics were deployed in BPA's synchrophasor laboratory for demonstration. The analytics were applied to 22 power plants of various types. The results presented here are based on 26 days of analysis in 2023. The frequency excursion detector performed well, but there is still a need to manually remove events that are not well-suited for analysis, such as instances where two excursions occurred in close sequence. The tool's user interface allows such events to be identified and removed easily. The results presented here include only

events that passed this review.

The findings from the field deployment showed that when viewed across the 26-day period, the FRM is an effective indicator of a plant's performance. Average FRM values for plants were dispersed fairly evenly from consistently negative to consistently positive. The results from two plants at opposite ends of this spectrum are presented in Fig. 11. Each point in the plot represents the response of a plant to a frequency excursion. As desired, Plant 2 consistently increased MW output following drops in frequency (lower-right quadrant) and decreased MW output following rises in frequency (upper-left quadrant). As a result, it had consistently large and negative FRM values. In contrast, Plant 1 did not respond to frequency excursions, so its reported change in MW output is small and essentially random. As a result, it had consistently positive FRM values.

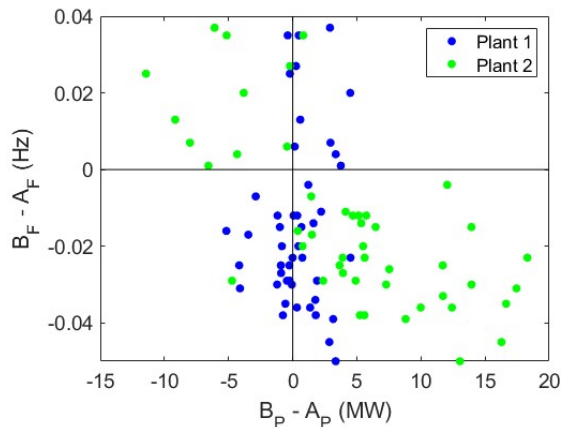


**Figure 11. Summary of responses from two power plants for all frequency excursions analyzed during the field demonstration. Plant 1 shows inconsistent performance, while Plant 2 regularly adjusts active power up for under-frequency excursions and down for over-frequency excursions.**

To further illustrate this difference in performance, the responses of the two plants are plotted for an under-frequency excursion in Fig. 12 and an over-frequency excursion in Fig. 13. For the under-frequency excursion, Plant 2 responds by outputting more MW, while for the over-frequency excursion it reduces its MW output. In contrast, Plant 1 is non-responsive.

## 5. VRM Results and Analysis

Results from the field demonstration also validated the VRM analysis approach proposed in Section 3. Though distinctions in plant performance were still

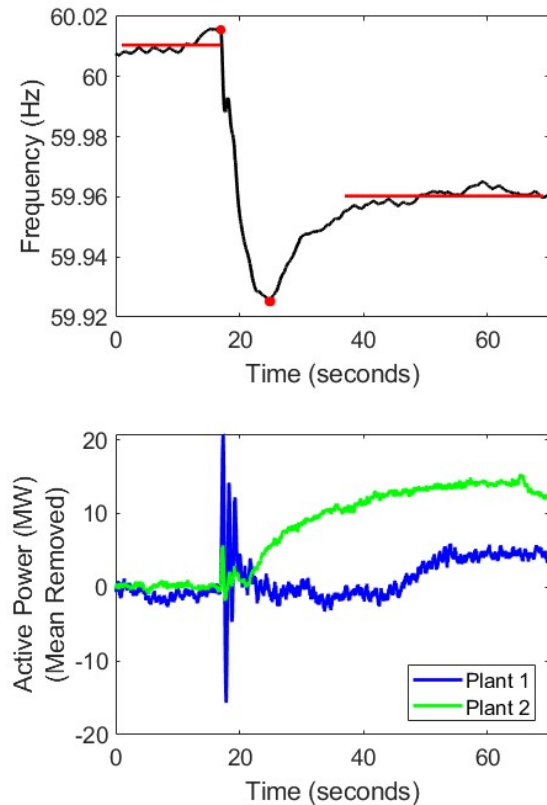


**Figure 12. An under-frequency excursion detected during the field demonstration (top) and the corresponding active power responses of two power plants (bottom).**

observable, the 22 power plants performed more consistently in terms of voltage response than frequency response. The full set of results is presented in Fig. 14.

As with the FRM results, unsuitable events were removed using the tool's user interface. Note that for almost all excursions, power plants responded with appropriate adjustments to reactive power output. As a result, the average VRM across the 26-day evaluation period was positive for all but one power plant, and that power plant's average was driven negative by a small number of events.

Though all power plants responded appropriately, there were notable differences in the scale of the response. For example, consider the responses of two plants to the same voltage excursion in Fig. 15. The response in MVAR output is much more significant for Plant 3 than for Plant 4 even though both the plants have headroom to provide MVAR support.

An additional finding from the field demonstration

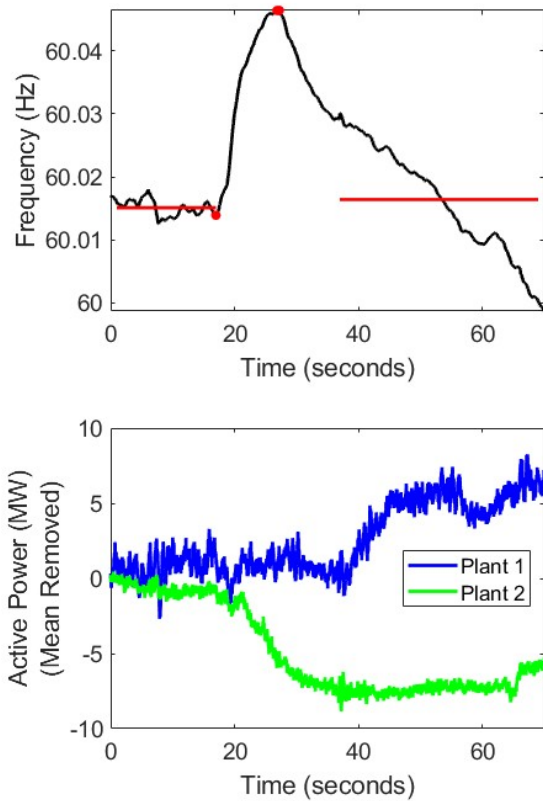


Figure 13. An over-frequency excursion detected during the field demonstration (top) and the corresponding active power responses of two power plants (bottom).

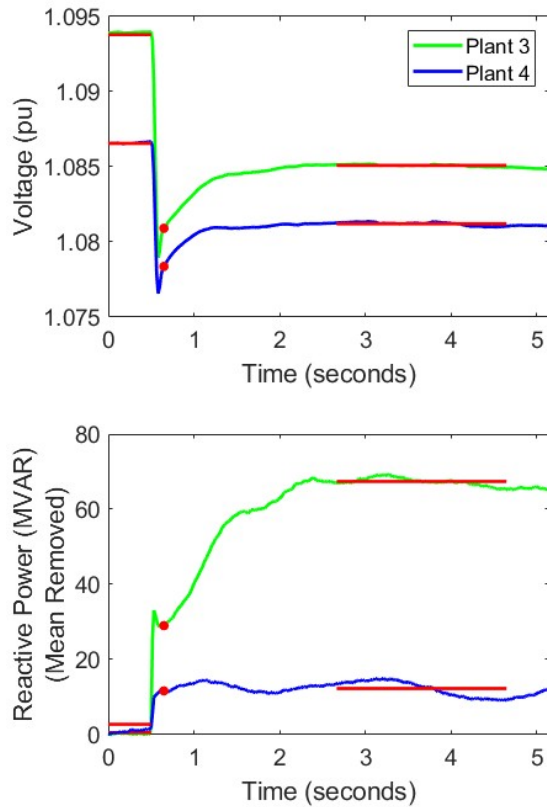


Figure 15. An under-voltage excursion detected during the field demonstration (top) and the corresponding reactive power responses of two power plants (bottom). Both plants increase reactive power output appropriately, with the response from Plant 3 being significantly stronger.

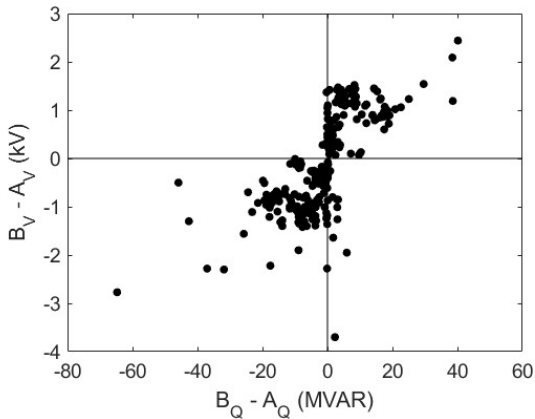


Figure 14. Summary of all voltage excursions analyzed during the field demonstration. Clustering in quadrants 1 and 3 indicate that plants across the territory appropriately adjusted reactive power.

is that the scaling terms in the denominator of (11) may need refinement. For almost all events the scaling terms serve their purpose, but there are cases when  $|C_Q - A_Q| \approx 0$ , leading to very large VRM values. This refinement will be an aspect of future work.

## 6. Conclusion

The results of the field demonstration at BPA validated the ability of the algorithms proposed in this paper to summarize the frequency and voltage control performance of power plants. These measurement-based summaries are useful in identifying plants for further review with model-based approaches.

There are several avenues for future work to make the methods more broadly applicable. First, the VRM formula (11) needs to be revisited to handle the

relatively rare cases where a very small reactive power scaling term causes the VRM to become quite large. A method for setting thresholds in the voltage excursion detector is also needed. The manual tuning used in this work was suitable for initial demonstration, but it may be challenging at scale. Finally, the filters used in the frequency excursion detector and start time estimator need to be retuned for other interconnections. One readily available opportunity is using frequency excursion events in the GESL repository to tune filters for the US Eastern Interconnection. With these aspects addressed, the methods proposed in this paper can be used by a broad set of utilities to effectively monitor the performance of power plants in their territory.

## Acknowledgment

The authors would like to thank Marissa Morales-Rodriguez of DOE's Solar Energy Technologies Office (SETO) and Sandra Jenkins of DOE's Office of Electricity for funding support and guidance. We are also grateful to our colleagues at LBNL, NREL, and ORNL for their contributions to the broader project.

## References

- [1] N. Hatziargyriou, J. Milanovic, C. Rahmann, V. Ajarapu, C. Canizares, I. Erlich, D. Hill, I. Hiskens, I. Kamwa, B. Pal, P. Pourbeik, J. Sanchez-Gasca, A. Stankovic, T. Van Cutsem, V. Vittal, and C. Vournas, "Definition and classification of power system stability – revisited & extended," *IEEE Transactions on Power Systems*, vol. 36, no. 4, pp. 3271–3281, 2021.
- [2] NERC. (2015) BAL-003-1 frequency response and frequency bias setting reliability standard. Atlanta, GA. [Online]. Available: <https://www.nerc.com/pa/Stand/Reliability20Standards/BAL-003-1.pdf>
- [3] NERC, "Standard MOD-027–1 - verification of models and data for turbine/governor and load control or active power/frequency," 2014.
- [4] NERC, "Standard MOD-026–1 - verification of models and data for generator excitation control system or plant volt/var control functions," 2014.
- [5] A. Phadke and J. S. Thorp, "History and applications of phasor measurements," in *2006 IEEE PES Power Systems Conference and Exposition*, 2006, pp. 331–335.
- [6] R. Quint, P. Etingov, D. Zhou, and D. Kosterev, "Frequency response analysis using automated tools and synchronized measurements," in *2016 IEEE Power and Energy Society General Meeting (PESGM)*, 2016, pp. 1–5.
- [7] P. Etingov, F. Tuffner, J. Follum, X. Li, H. Wang, R. Diao, Y. Zhang, Z. Hou, Y. Liu, D. Kosterev, S. Yang, and G. Matthews, "Open-source suite for advanced synchrophasor analysis," in *2018 IEEE/PES Transmission and Distribution Conference and Exposition (T&D)*, 2018, pp. 1–5.
- [8] C. Lackner, J. H. Chow, and F. Wilches-Bernal, "Performance evaluation of STATCOM equipment using ambient and disturbance data," in *2019 IEEE Milan PowerTech*, 2019, pp. 1–5.
- [9] F. Wilches-Bernal, C. Lackner, and J. H. Chow, "Model reduction of wind turbine generator models for control performance evaluation," in *2020 IEEE/PES Transmission and Distribution Conference and Exposition (T&D)*, 2020, pp. 1–5.
- [10] J. Follum, P. Mana, and E. Mitchell-Colgan. (2024, Apr.) Field demonstration of an automated generator evaluation tool at BPA. [Online]. Available: <https://www.naspi.org/node/981>
- [11] Y. Liu, H. Li, E. Zhan, and C. Chen. (2023, Apr.) Realtime inertia monitor based on pumped hydro operation signatures. [Online]. Available: <https://www.naspi.org/node/963>
- [12] P. Etingov, J. Follum, S. Biswas, and T. Yin, "Open source synergy: Developing and validating PMU data analysis techniques using open source tools and datasets," in *Smart Grid Synchronized Measurements and Analytics (SGSMA)*, 2024.
- [13] Oak Ridge National Laboratory, Lawrence Livermore National Laboratory, Pacific Northwest National Laboratory, "Grid Event Signature Library," 2022. [Online]. Available: <https://gesl.ornl.gov>
- [14] S. Biswas, J. Follum, P. Etingov, X. Fan, and T. Yin, "An open-source library of phasor measurement unit data capturing real bulk power systems behavior," *IEEE Access*, vol. 11, pp. 108 852–108 863, 2023.
- [15] "Primary frequency control reliability guideline," North American Electric Reliability Corporation (NERC), Tech. Rep., 2019.
- [16] Modeling and Validation Work Group (MVWG), "WECC second generation wind turbine models," 2014. [Online]. Available: <https://www.wecc.org/Reliability/WECC-SecondGeneration-Wind-Turbine-Models-012314.pdf>